

Validation of an experimental technique with the physically based global method

Jacek Magiera

Cracow University of Technology, Dept. of Civil Engineering

Institute for Computational Civil Engineering, Warszawska 24, 31-155 Cracow

e-mail: plmagier@cyf-kr.edu.pl

Validation of an experimental approach requires that both model and data errors are proved to be within acceptable ranges. In case of destructive testing none of the classic, statistically based methods can be applied for that task due to the lack of independent data series required for building data statistics. The aim of the paper is to present a non-statistical methodology for performing such validation, developed within the framework of physically based approximation (PBA). It has been developed to validate a neutron diffraction based experimental-numerical approach applied for studying 3D rail residual stress. It is for the PBA technique's capability to provide high quality physically reasonable data fits for one data set only, treated here as higher order reference fields that made it possible to develop this methodology and perform error analysis/validation. In many ways this approach is analogical to Zienkiewicz-Zhu type of error estimators, and its performance will be demonstrated for a defective RE136 rail sample that was installed in a US DOT test track.

Keywords: physically based approximation, experimental data error estimation, validation of experimental technique, residual stress in railroad rails, neutronography.

1. INTRODUCTION

Results of experimental investigations are usually not exact, not only because of random errors that occur during experiments but also due to shortcomings of the models of the investigated phenomena used for constructing the solution. Nowadays, it is a common practice that once the experimental data is collected, it is then processed by advanced numerical routines that are based on theoretical models. In this case the quality of the final results and validity of the approach depend on both the quality of the collected data and validity (correctness) of assumptions adopted for the considered model. It comes to no surprise, though, that in order to build effective solution procedures, the underlying assumptions are often taken as simple as possible, which gives the convenience of calculations speed-up and simplifies computer codes. However, it may also give an unplanned outcome: loss of the data quality and/or validity of the final results, should the model simplifications be pushed somewhat beyond the physics of the examined phenomena. Destructive testing may further undermine data credibility, because once destroyed, the specimens cannot be examined repetitively for a number of times to collect independent data sets, then build data statistics, perform error analysis and enhance/smooth the data (evaluate and correct errors). In that case the “as-is” data used for the subsequent numerical modeling/processing may be a source of substantial level of error that will bias the final results. This error will have two components: data error (usually random) and model error (usually permanent) – and at this stage it will be extremely hard to separate these two types of errors and to evaluate their magnitudes. This may void the chance to judge whether the model – and the assumptions that laid foundation for it – were legitimate.

The above considerations exactly reflect a real problem, where the need for such a validation analysis was faced. It occurred when a new method for experimental examination and numerical

reconstruction of the 3D rail residual stress was proposed [1]. This new technique was called T/O-S, which stands for “Transverse/Oblique Slicing” technique. Its idea was W. Karmowski’s creative development of the classic destructive schemes worked out in several independent US research centers in the 1980s and employed many times [2–4]. These methods shared several common ideas. One of them was application of practically the same trepanation scheme that required sectioning of a rail slab into two samples: a relatively thin transverse slice, which was subsequently – after strain gauge instrumentation – cut into small cubes (for 2D in-plane strain measurements), and quite a long, ca. 0.3–0.5 m so-called Meier section (adopted after Meier’s original work [5]), which was in turn cut into rods corresponding to the cubes (to determine the change of the 1D axial strain). The original 3D stress distribution was obtained by an algebraic-type data reduction procedure, pretty simple thanks to the assumptions that the stress state was independent of the axial coordinate and there were no active plastic processes present when the dicing/Meier section took place.

The T/O-S scheme (Fig. 1) was similar to the above methods in that it also required that the rail is cut into two specimens, one of which was exactly the same transverse slice, while the other was an oblique slice cut under some angle with respect to the axial direction, and the two basic assumptions of the old techniques were adopted, too. The fundamental difference was that this time Meier sectioning, providing 1D data was replaced by a second inclined slice, which provided 2D data for in-plane strains/stresses. J. Orkisz showed theoretically and J. Magiera numerically [1, 6, 7] that based on this data it is possible to reconstruct the original, undisturbed by cutting, 3D residual stress as it used to exist in the uncut rail slab.

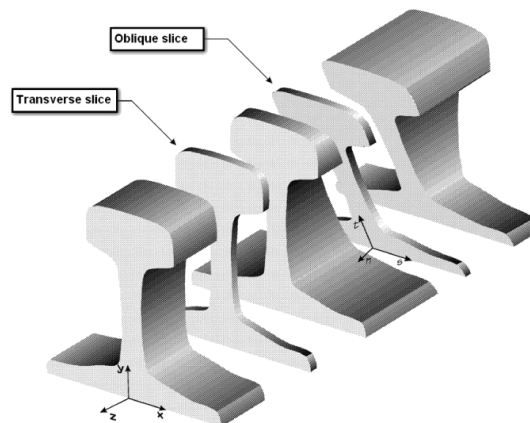


Fig. 1. Classic Transverse/Oblique Slicing technique.

Even though the T/O-S sectioning scheme brought an overall time- and cost-efficiency improvement¹, it created concerns about its validity for the case of railroad rails. The weak point was the fundamental assumption about the independence of the stress state of the axial coordinate Z (see Fig. 1 for notations). What hides behind this assumption is the idea of treating rails as truly prismatic bodies. In reality, it is questionable due to the nature of the conditions rails work in. The discrete (periodic) support of the ties installed in the track makes some cross-sections of rails (those lying on a tie) to work under purely compressive, contact-type loading while the cross-sections lying between the ties are additionally subject to seemingly strong bending. And there may be other effects like varying track curvature (on arcs), off-center wandering of the contact patch due to different lateral forces, wheel imperfections, etc., which could make the stress state in rails far from the ideal “prismatic” state postulated in the fundamental assumption. For the older techniques [2–4] it was not a big problem: the averaging nature of Meier sectioning prevented those approaches from bigger divergences. But the case of the T/O-S technique is different, because here fulfillment of the

¹Which was the driving force for its development; sectioning the Meier part into rods under a strict regime was a very time-consuming and expensive procedure.

fundamental assumption becomes critical. It is so because if the stress state did not conform to the fundamental assumption, the oblique slice would be spanning over cross-sections of varying stress state. After removing from the rail slab it would not be in a 2D stress state as assumed, but in a more complex 3D stress state, with out-of-plane shear stress components present. Without an a priori knowledge of how the stress state varies along the axial coordinate, those effects would be totally out of control. If they were neglected, the 3D stress reconstruction routine would lead to final results biased by errors of unknown amplitude, probably making them worthless.

In order to investigate the problem and to prove that the fundamental assumption holds, a new N-cut² sectioning scheme was proposed [8]. This new scheme requires that an additional transverse slice is cut in a manner that the oblique slice resides between two transverse slices – see Fig. 2. Such a setup makes it possible to build error measures suitable for performing the validation analysis.

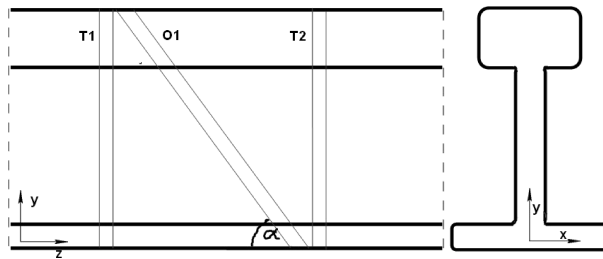


Fig. 2. New N-cut rail sectioning scheme. Side view.

The key technique for the validation analysis proposed here is the physically based global method [6, 7] (called in short PBGM), a version of the PBA general approach [9]) used as a physically reasonable³ preprocessing technique for enhancement (smoothing) of raw 2D experimental data. Thanks to its ability to provide non-statistical a posteriori estimates of the experimental data error [10–12], the PBGM technique makes it possible to separate the data error from the model error – and if the latter is found negligible, then to validate the approach.

It is important to emphasize here that the PBGM method may work on a single data set only and still will be capable of providing error estimates without any statistical inference. This is a truly unique feature of the PBGM approach, competitive with classic statistical approaches, faster and more cost-effective due to minimalist requirements in what regards the number of the required data sets or lab/data reduction time.

2. PHYSICALLY BASED GLOBAL METHOD

The global method of the physically based approximation is a two-stage non-linear constrained optimization problem formulated as [9]:

Stage I. Find self-equilibrated field $\sigma(xy)$ realizing stationary point of $\Phi(\sigma, \lambda)$:

$$\min_{\sigma} \Phi(\sigma, \lambda) = \lambda \Phi^T(\sigma) + (1 - \lambda) \Phi^E(\sigma), \quad (1)$$

where Φ^T is the theoretical part and Φ^E is the experimental part of the hybrid functional $\Phi(\sigma, \lambda)$, σ is the stress tensor⁴ and λ is a weighting parameter, respectively. The stationary point of (1) is sought with the following constraints imposed:

local equilibrium equations⁵:

$$\sigma_{ij,j} = 0 \quad \text{in } A, \quad \sigma_{ij} n_j = 0 \quad \text{on } \partial A \quad (2)$$

²It was called “N-cut scheme” owing to the resemblance of the letter N the slices form when looked from a side.

³i.e., the fits to the data follows laws/requirements that comes from the physics of the phenomena.

⁴Dimensionless stress, to be exact.

⁵Equilibrium equations are written here in the form valid for the self-equilibrated stress state.

and global equilibrium equations⁶:

$$\int_A \sigma_{xx} dA = 0, \quad \int_A \sigma_{yy} dA = 0, \quad \int_A [(\sigma_{xx} + \tau_{yx})y - (\sigma_{yy} + \tau_{xy})x] dA = 0. \quad (3)$$

In addition to the constraints of theoretical roots (2)–(3), there are also imposed constraints that come from the experimental side. They express a request that the approximated (i.e., smoothed) field $F(\bar{\sigma}_{ij}^k)$ at the k -th experimental point location be within the allowable error tolerances, denoted here as local $\Delta F(\sigma_{ij}^k)$ and global $\Delta F_{\text{global}}(\sigma_{ij})$ error tolerances, respectively, as compared to the original measurements $F(\sigma_{ij}^k)$. Those constraints are in the form of inequalities, and may count local:

$$|F(\sigma_{ij}^k) - F(\bar{\sigma}_{ij}^k)| \leq \Delta F(\sigma_{ij}^k), \quad i, j = 1, 2, \quad k = 1, K, \quad (4)$$

and global types of constraint:

$$\sqrt{\frac{1}{K} \sum_{k=1}^{K_m} \frac{(F(\bar{\sigma}_{ij}^k) - F(\sigma_{ij}^k))^2}{\Delta F(\sigma_{ij}^k)^2}} \leq \Delta F_{\text{global}}(\sigma_{ij}), \quad i, j = 1, 2, \quad k = 1, K. \quad (5)$$

In Ineq. (4)–(5), $k = 1$ to K enumerates the experimental data points and $F()$ is the function that maps stress subspace to the subspace of original measurements (e.g., strains)⁷. The theoretical part $\Phi^T(\sigma)$ of the hybrid functional (Eq. (1)) was chosen as the global Karmowski's tensor curvature [9, 13]:

$$\Phi^T = \frac{1}{V} \int_V \kappa^2(\sigma_{ij}) dV = \frac{1}{2\pi} \frac{1}{V} \int_V \int_0^{2\pi} \frac{\partial^2 \sigma_{ij}}{\partial \nu^2} \frac{\partial^2 \sigma_{ij}}{\partial \nu^2} d\phi dV \quad (6)$$

and the experimental part $\Phi^E(\sigma)$ as a classic variance-type formula:

$$\Phi^E(\sigma) = \frac{1}{3K} \sum_{i,j=1}^2 \sum_{k=1}^K \left(\frac{F(\sigma_{ij}^k) - F(\check{\sigma}_{ij}^k)}{\Delta F(\sigma_{ij}^k)} \right)^2, \quad i, j = 1, 2, \quad k = 1, \dots, K. \quad (7)$$

Stage II. Find

$$\max \lambda, \lambda \in [0, 1] \quad (8)$$

for which inequalities (4)–(5) still hold at all nodes.

From the numerical point of view the process of arriving at the final solution is iterative. Parameter λ starts from 0 (at that point Ineq. (4)–(5) are not violated) and is augmented to such a λ_{max} for which the solution to the Stage I problem (Eqs. (1)–(3)) will satisfy any of the constraints (4)–(5) at a point.

The PBGM approach was subject to profound testing for simulated and real experimental data [6, 10–12]⁸ and its stability and performance was confirmed.

⁶Eqs. (3) express a request that total forces acting in the X , Y directions as well as the total torsion in the Z -axis direction are equal to naught (holds for the self-equilibrated stress state).

⁷In our case, accordingly to the assumption taken that the stress relief process that occurs during sectioning is purely elastic, it is justifiable to adopt Hook's law here.

⁸And numerous reports the author submitted to US DOT, FRA in years 1992–2005.

3. VALIDATION OF THE T/O-S TECHNIQUE WITH THE NEW N-CUT SECTIONING SCHEME AND THE PBGM APPROACH

As presented, the transverse/oblique slicing procedure [1] is a special arrangement of destructive rail specimen extraction, accompanied by a dedicated numerical algorithm that serves to reconstruct the original 3D rail residual stress. It was also stressed that in case of the T/O-S technique it is critical that the stress state does not change along the axial coordinate. In the original T/O-S sectioning scheme, validity of this assumption was taken for granted⁹, but now it was proposed to monitor it on the run-time by application of a new, extended sectioning scheme. It will be discussed now how cutting of an additional transverse slice turns the former two-slice T/O-S method into a new technique that has built-in provisions for self-monitoring, including model validity check.

In fact, there are many techniques that might be applied to check whether the stress state is conforming to the assumptions taken, to mention only ultrasound or EMAT scanning. But what can be done with these techniques is usually limited to subsurface layers and they are very sensitive to texture, material properties and composition change, which often happens in case of rails [14] due to extreme amplitudes of the loading. Moreover, these techniques depend on some material constants – but different from the ND technique¹⁰ – so the results they would give might be somehow biased as compared to the ND technique, and thus the reasoning based on those “external” results could be inconsistent. The N-cut scheme is compatible with the T/O-S experiment methodology, it is based on the same detecting philosophy and the same material constant – so it is an “internal” technique which guaranties “consistent reasoning”.

Let us discuss now briefly the add-ons the N-cut scheme brings to the already worked out experimental setup. As already mentioned, in this new setup (Fig. 2) in addition to extracting the T1 and O1 slices, which form the classic two-slice T/O-S scheme, a second transverse slice is extracted, denoted here as T2 slice. If the oblique slice is cut at an inclination angle $\alpha = 45^\circ$, the T2 slice will be ca. 0.18–0.20 m distant from the T1 transverse slice¹¹, which will form a good base for the analysis of the behavior of the stress state along the axial coordinate Z .

So, if the experiments are performed according to the N-cut scheme, they will provide the following three data sets:

1. in-plane stress components on the T1 slice: $\bar{\sigma}'_{xx}$, $\bar{\sigma}'_{yy}$ and $\bar{\sigma}'_{xy}$,
2. in-plane stress components on the T2 slice: $\bar{\sigma}''_{xx}$, $\bar{\sigma}''_{yy}$ and $\bar{\sigma}''_{xy}$ and
3. in-plane stress components on the O1 slice: $\bar{\sigma}_{ss}$, $\bar{\sigma}_{tt}$ and $\bar{\sigma}_{st}$,

where $\bar{\sigma}_{ij}$ denotes the stress state disturbed by slice removal (in-plane stress components of the original stress state in the slices were subject to partial stress relief when the normal stresses were totally relieved).

Theoretically, if the experiment is error free (lack of data error) and the assumption about the independence of the stress state of the axial coordinate is valid (lack of model error), the data sets for T1: $\bar{\sigma}'_{ij}$ and T2: $\bar{\sigma}''_{ij}$, $i, j = 1, 2$ will be exactly the same. If they are not – and this is what is seen in the real case due to errors – the discrepancies may be attributed to both data error or model error. The point is to separate these errors and tell what their respective amplitudes are, then to check whether the model error is sufficiently low to be neglected.

⁹In fact, the original version was conceived for analysis of rails tested in the EMS-60 testbed, a facility built at the Railway Scientific and Technical Center of the Polish State Railroads. The EMS-60 machine provided continuous support for the tested rails, the samples were straight, the loading was applied on the same central part of the running thread so the samples were truly in the plane strain state and there was no place for stress state fluctuations along the axial coordinate. Moreover the in-plane stress distributions were symmetric in that case.

¹⁰These constants, too, will have to be determined somehow, adding to the cost and time of experiments.

¹¹The most common rail heights are in the 0.17–0.18 m range, so for an oblique slice cut at 45° inclination angle the distance between the T1 and T2 slices will be exactly the same, save for a few millimeters extra to make room for the saw blade.

The procedure is based on the physically based global method. Having two independent data sets collected on the transverse slices T1 and T2 at two distant cross-sections of the rail, there are several things that may be done to check whether the stress state falls within the limits that were assumed about its behavior.

First of all, the component-by-component differences between the T1 and T2 raw data may be calculated and plotted:

$$\Delta\bar{\sigma}'_{ij}{}'' = \left| \bar{\sigma}'_{ij} - \bar{\sigma}''_{ij} \right|, \quad ij = 1, 2. \quad (9)$$

Secondly, the raw data for the stress components may be averaged, and based on these averages, maps of the prior-to-smoothing data error estimates for the T1:

$$\Delta\bar{\sigma}'_{ij} = \left| \bar{\sigma}_{ij}^{avg} - \bar{\sigma}'_{ij} \right|, \quad ij = 1, 2, \quad (10)$$

and T2:

$$\Delta\bar{\sigma}''_{ij} = \left| \bar{\sigma}_{ij}^{avg} - \bar{\sigma}''_{ij} \right|, \quad ij = 1, 2 \quad (11)$$

slices may be calculated and plotted. The averaged values themselves:

$$\bar{\sigma}_{ij}^{avg} = \frac{1}{2} \left(\bar{\sigma}'_{ij} + \bar{\sigma}''_{ij} \right), \quad ij = 1, 2 \quad (12)$$

may also be treated as raw data collected on a “virtual” averaged *Tavg* transverse slice, on the assumption of higher accuracy¹². If the discrepancies between the T1 and T2 data sets are of random origins, the *Tavg* data should be visibly smoother. One may also try to qualitatively analyze whether the variations of the raw T1 and T2 data for the individual stress components form any spatially repeatable patterns. Let us assume, for instance, that one analyzes the differences between horizontal stress on both slices $\Delta\bar{\sigma}'_{xx}{}''$ (Eq. (9)) over the cross-section of the rail and this relation is described by a function $\mathcal{F}(x, y)$:

$$\Delta\bar{\sigma}'_{xx}{}''(xy) = \mathcal{F}(x, y). \quad (13)$$

If the stress state is constant along the axial coordinate, and – in an ideal case – the data error equals zero, the same function $\mathcal{F}(x, y)$ will also describe relations for the remaining two stress components:

$$\begin{aligned} \Delta\bar{\sigma}'_{yy}{}''(x, y) &= \mathcal{F}(x, y), \\ \Delta\bar{\sigma}'_{xy}{}''(x, y) &= \mathcal{F}(x, y) \end{aligned} \quad (14)$$

and identically equal zero: $\mathcal{F}(x, y) \equiv 0$.

In the real case, however, the data will be biased by an error and hence the function will not identically equal zero: $\mathcal{F}(x, y) \neq 0$ – so the plots of the stress component differences defined by Eq. (9) will differ, as if there were three functions: $\mathcal{F}_1(x, y)$, $\mathcal{F}_2(x, y)$ and $\mathcal{F}_3(x, y)$. If those distributions across the rail cross-section would be spatially totally different, it might be a good indication that they represent purely random error (i.e., data error), not the systematic error (i.e., model error). On the other hand, if the functions: $\mathcal{F}_1(x, y) \neq 0$, $\mathcal{F}_2(x, y) \neq 0$ and $\mathcal{F}_3(x, y) \neq 0$, but they shared a visible similarity in their spatial distributions, it would be a strong point to support the thesis that this happens due to the presence of the model error, which means that there is a stress state change along the axial coordinate. In that case the T/O-S procedure will not provide credible results for 3D stress.

¹²True only if there is no stress state change along the axial coordinate.

The above options were considered for raw data, but one may have difficulty to infer valid conclusions in this case because the ND technique gives sometimes quite noisy data and the analysis of the difference patterns like those in Eq. (9) for raw data may be ineffective. But the same analysis may be performed for the PBGM-smoothened data. In this case the data will be smooth and the trends clearly visible. In this case even broader options exist, because the T1 and T2 data, after they are PBGM-smoothed independently, may be averaged to build a “higher order” reference field. On the other hand, one may also smooth the *Tavg* “virtual” slice data of Eq. (12). Because the *Tavg* data, as average, was supposedly of higher accuracy¹³, the PBGM-smoothed *Tavg* data should also be of higher accuracy than the separately smoothed T1 or T2 data. Therefore, if it is proved that the smoothed and then averaged T1, T2 slices data when compared to the smoothed *Tavg* data are almost the same (save for some minor, negligible differences justified by the random processes present), it will also be proved that the operations of smoothing and averaging are interchangeable and the final results are independent of data-reduction-path. In other words, if the “average-then-smooth” and the “smooth-then-average” processes produce the same (or almost the same) result, this would simply mean that the experimental error is limited to random error only¹⁴. Should the systematic (model) error be present, the resultant fields of “average-then-smooth” and “smooth-then-average” processes would be different.

And, similarly to the raw data case, one may be also interested in performing an analysis of the spatial distribution of differences between the smoothed T1 and T2 data. These variations would be expressed by analogy to Eq. (9) as:

$$\Delta\bar{\sigma}'_{ij'PBGM} = \left| \bar{\sigma}'_{ij'PBGM} - \bar{\sigma}''_{ij'PBGM} \right|, \quad ij = 1, 2. \quad (15)$$

If the spatial distributions of the $\Delta\bar{\sigma}'_{ij'PBGM}$ for the horizontal, vertical and shear stress components are different from each other and their amplitudes are reasonably low, one may treat the model error as negligible.

4. VALIDATION RESULTS

The results of the validation procedure for the N-cut T/O-S data will be presented here, due to scarcity of place the discussion will be held mainly for the horizontal stress component – as a representative. Examples of data used for this analysis were collected for a defective rail taken out of the test track loop of the US Department of Transportation, Transportation Technology Center (TTC), Pueblo, CO. This rail was scanned for residual stress by the neutron diffraction technique at the National Institute for Standards and Technology (NIST), US Department of Commerce, Gaithersburg, MD. Experiments were performed at the NIST’s atomic reactor facility with neutron radiation from a steady state reactor, generating stream of neutrons with wavelengths of $\lambda \approx 1.68 \text{ \AA}$. The samples were exposed to a beam that was cut down in size by neutron absorbing apertures to a final probing volume of ca. $2 \times 2 \times 2 \text{ mm}^3$.

The raw results for the analyzed rail are shown in Fig. 3 for the $\bar{\sigma}'_{xx}$ stress on T1 slice and in Fig. 4 for the $\bar{\sigma}''_{xx}$ stress on T2 slice, respectively. They bear quite good resemblance to each other, though there is some noise that pollutes the fields. Calculation of the raw average stress on the “virtual” *Tavg* slice (Eq. (12)) produces the patterns of the $\bar{\sigma}^{avg}_{xx}$ stress shown in Fig. 5 – qualitatively slightly smoother than the T1 and T2 patterns (compare respective columns with maximum error norms in Table 1).

¹³Valid when the experimental data error is assumed to have normal distribution.

¹⁴PBGM smoothing is based on minimization of the Karmowski’s tensor curvature – Eq. (6). In this process (which goes in parallel to simultaneous enforcement of physical relations like equilibrium conditions), the high-frequency/high amplitude experimental data error is curbed in the first place. Consequently, if the stress state on the T2 slice was different from the state on slice T1, PBGM smoothing would smooth it to its own physically admissible state, different from the T1 slice and this would be clearly visible in the plotted maps.

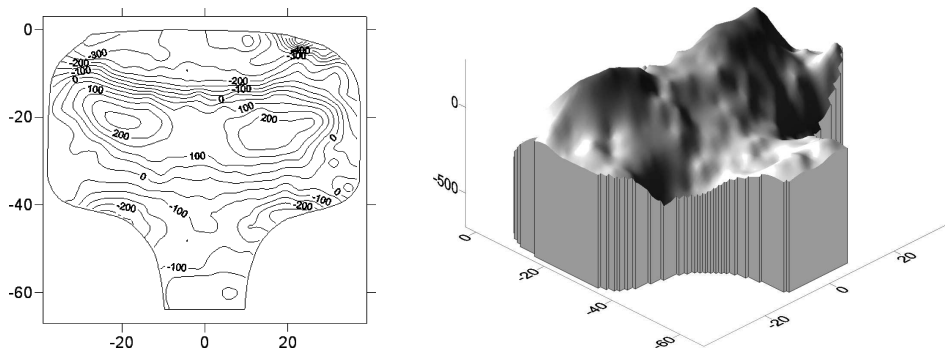


Fig. 3. Horizontal stress σ_{xx} for T1 slice – raw data.

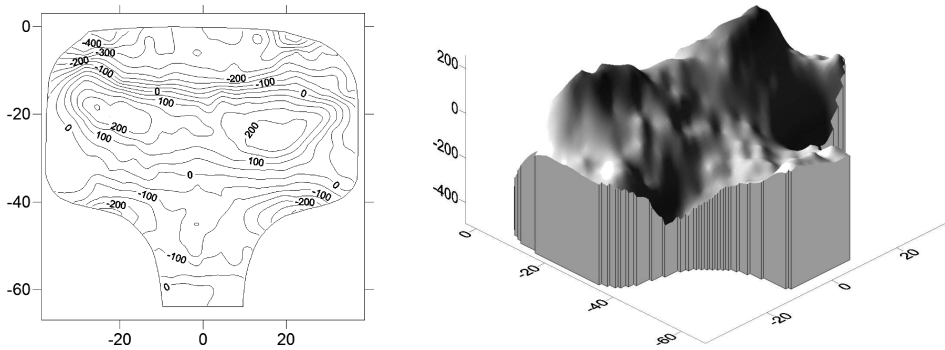


Fig. 4. Horizontal stress σ_{xx} for T2 slice – raw data.

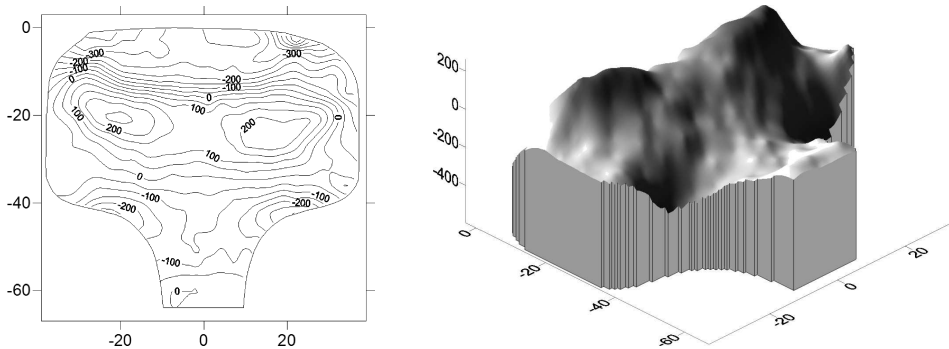


Fig. 5. Horizontal stress σ_{xx} for T_{avg} virtual slice – raw data.

Table 1. Maximum and L_2 norms for the raw data.

Stress component	Error norms for raw T1 slice data $\ \sigma'\ $		Error norms for raw T2 slice data $\ \sigma''\ $		Error norms for raw T_{avg} “virtual” slice data $\ \frac{1}{2}(\sigma' + \sigma'')\ $	
	Max. [MPa]	L2	Max. [MPa]	L2	Max. [MPa]	L2
σ_{xx}	698.68	27697.89	491.34	27165.94	595.65	27290.02
σ_{xy}	345.04	8106.454	239.57	7310.02	231.20	7466.31
σ_{yy}	516.16	21099.07	516.77	20946.75	449.95	20786.15

Calculation of the component-by-component differences between the T1 and T2 data (Eq. (9)) provides the patterns shown in Figs. 6–8. Because they represent distributions of the functions: $\mathcal{F}_1(x, y)$, $\mathcal{F}_2(x, y)$ and $\mathcal{F}_3(x, y)$ – Eq. (13)–(14) – and their mutual similarity/dissimilarity will serve for a qualitative-type validation analysis, all three components data were recalled here. Even

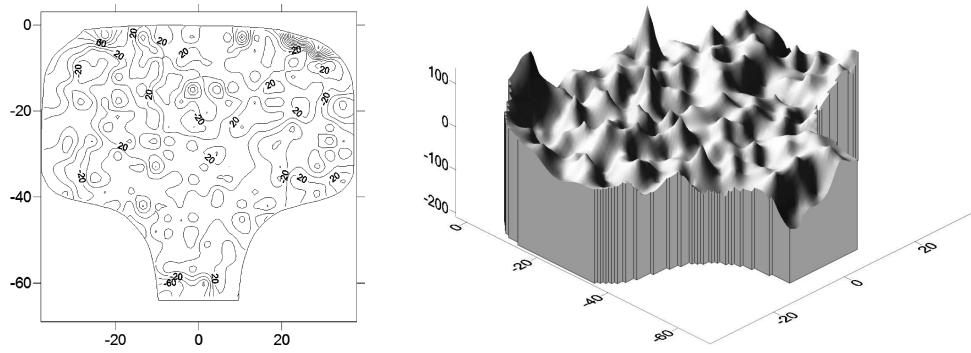


Fig. 6. Differences between horizontal stresses σ_{xx} on T1 and T2 slices – raw data.

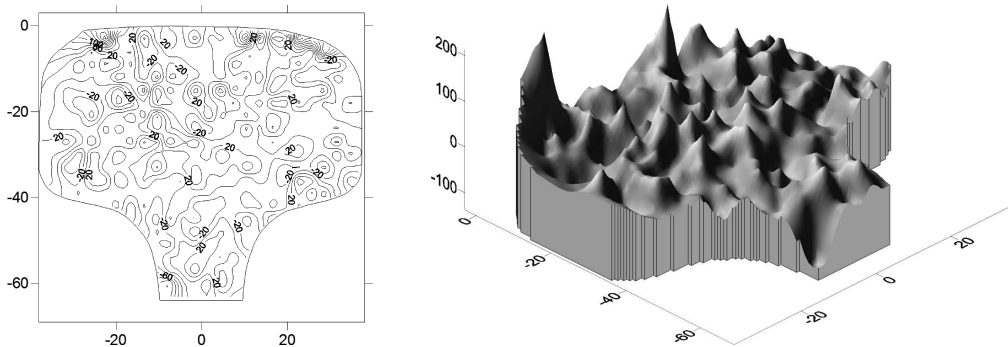


Fig. 7. Differences between vertical stresses σ_{yy} on T1 and T2 slices – raw data.

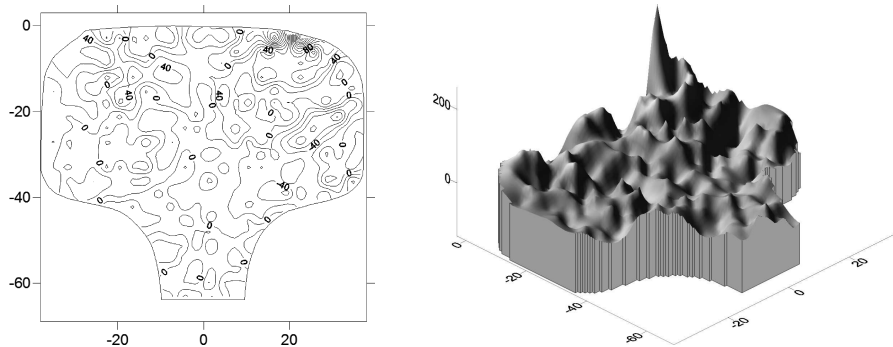


Fig. 8. Differences between shear stresses σ_{xy} on T1 and T2 slices – raw data.

a cursory look at these patterns reveals them to be very noisy and that on average their amplitudes are within the ± 100 MPa range. At some regions, however, they may reach even a 200 MPa range. At this level of noise it is difficult to judge whether these patterns are really similar to each other or not. Definitely, they are not close to zero and without smoothing the concept of seeking similarities between the $\mathcal{F}_1(x, y)$, $\mathcal{F}_2(x, y)$ and $\mathcal{F}_3(x, y)$ can hardly be applied. To provide more objective measures, maximum and L_2 error norms were computed to find estimates of the error. Definitions are classic, like in the Eqs. (16)–(17):

$$\left\| \Delta \bar{\sigma}'_{ij} \right\|_{\max} = \max_{(x,y)} \left| \bar{\sigma}'_{ij} - \bar{\sigma}''_{ij} \right|, \quad ij = 1, 2, \quad (16)$$

$$\left\| \Delta \bar{\sigma}'_{ij} \right\|_{L_2} = \frac{1}{A} \int_A \left(\bar{\sigma}'_{ij} - \bar{\sigma}''_{ij} \right)^2 dA, \quad ij = 1, 2. \quad (17)$$

Here they are written for difference-type quantities $\Delta \bar{\sigma}'_{ij}$ defined in Eq. (13), but these formulas will also be used for computing norms of the stress components themselves. The results for the

error norm analysis for raw data are collected in Table 1. As can be seen, the discrepancies between the two raw data sets are huge, especially visible in the maximum error norm terms (again, the previously reported value of ca. 200 MPa is found). Analysis of the error plots in Figs. 6–8 makes it possible to conclude that these big errors happen to occur only at isolated data points very close to the railhead boundaries. This is a behavior observed in all ND data sets and comes to no surprise, as these are the areas where material constants might be subject to biggest change due to extreme loading amplitudes. The L_2 error norm is more stable for T1, T2 and T_{avg} data sets, which means that on average they are comparable, and no systematic shift in the values of these norms for T1 and T2 slices may be spotted. Internal parts of the railhead area do exhibit some fluctuations, but they are of minor importance.

PBGM smoothing results for the σ_{xx} stress component are shown in Figs. 9–11. As can be seen, this stress field component has now smooth representations and the T1, T2 and T_{avg} patterns are visually very much the same. Analysis of the error norms in Tables 2–4, however, reveals that there are still places where the error remains on a substantial level. In fact, the differences between the stress components before and after PBGM smoothing expressed by maximum error norm (see e.g., data for transverse stress in columns 1 and 3, Table 2) remained almost untouched (again, ca.

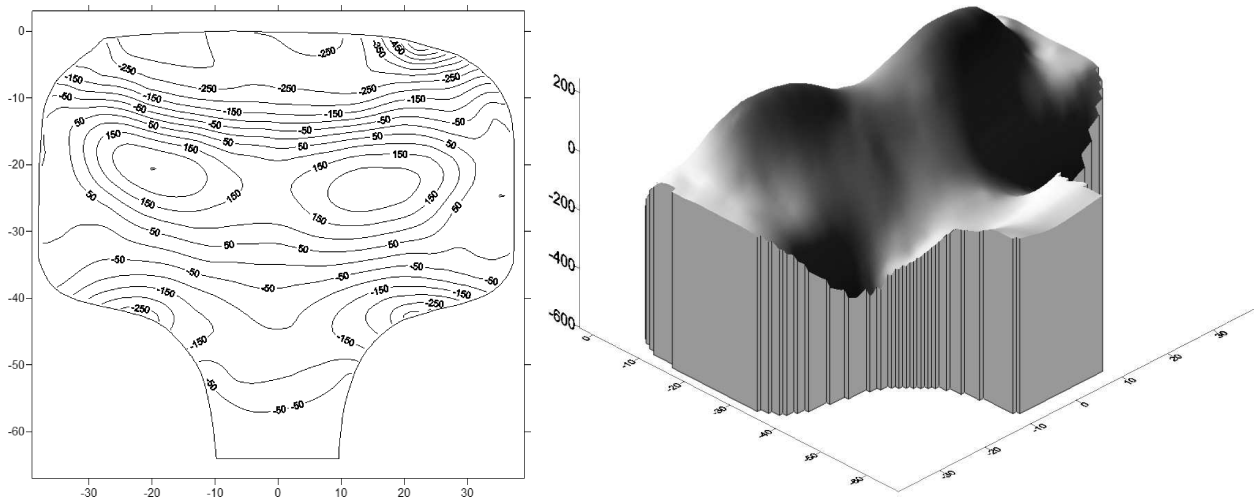


Fig. 9. Horizontal stress σ_{xx} for T1 slice – PBGM-smoothed data.

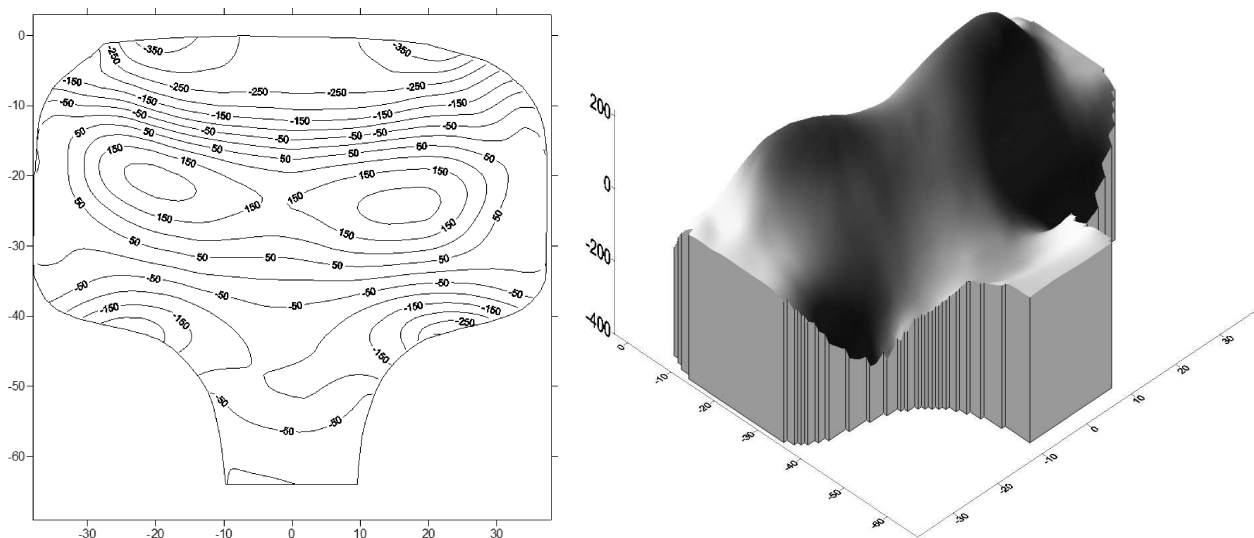


Fig. 10. Horizontal stress σ_{xx} for T2 slice – PBGM-smoothed data.

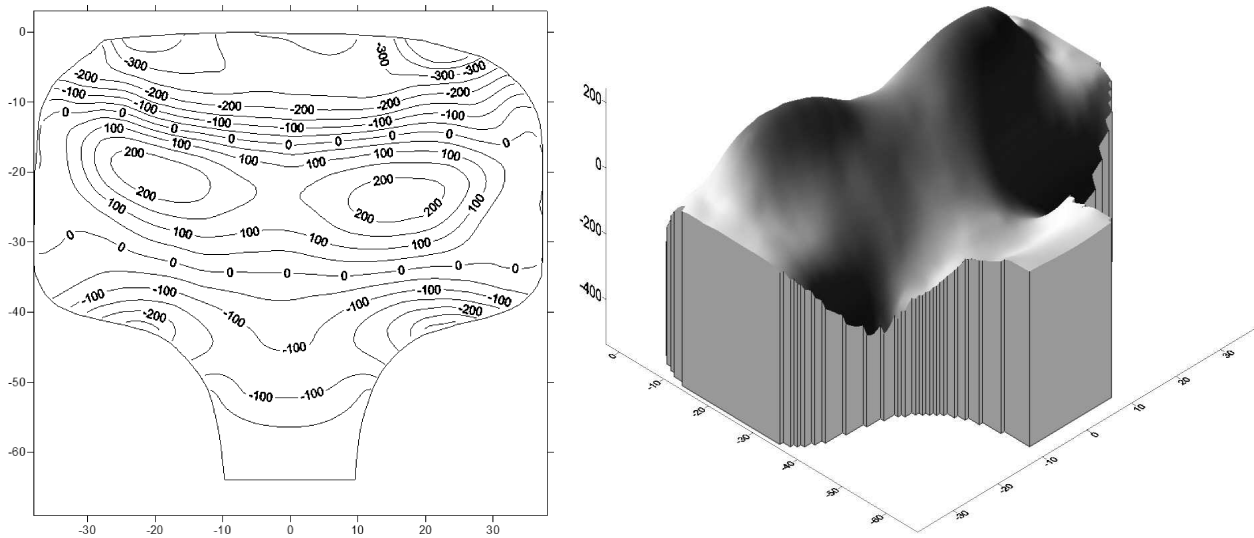


Fig. 11. Horizontal stress σ_{xx} for T_{avg} virtual slice – PBGM-smoothed data.

Table 2. Maximum and $L2$ norms for the differences between T1 and T2 slices for raw and PBGM-smoothed data.

Error norms for T1 and T2 raw data differences $\ \bar{\sigma}'_{ij} - \bar{\sigma}''_{ij}\ $		Error norms for T1 and T2 PBGM-smoothed data differences $\ \bar{\sigma}'_{ij'PBGM} - \bar{\sigma}''_{ij'PBGM}\ $	
Max. [MPa]	L2	Max. [MPa]	L2
208.97	723.89	208.83	402.64
260.27	928.78	57.69	354.46
213.21	931.25	120.35	391.52

Table 3. Maximum and $L2$ error norms for the PBGM-smoothed data.

Stress component	Norms for PBGM-smooth. T1 slice data $\ \sigma'_{PBGM}\ $		Norms for PBGM-smooth. T2 slice data $\ \sigma''_{PBGM}\ $		Norms for PBGM-smooth. T_{avg} slice data $\ \sigma^{avg}_{PBGM}\ $		Norms for averaged PBGM-smoothed T1 and T2 slice data a^*		“Average-then-smooth” vs. “Smooth-then-average” error norms a^{**}	
	Max. [MPa]	L2	Max. [MPa]	L2	Max. [MPa]	L2	Max. [MPa]	L2	Max. [MPa]	L2
σ_{xx}	606.43	24573.30	397.50	22089.72	530.94	24308.97	523.88	24168.38	7.06	1.26
σ_{xy}	189.15	5408.93	156.97	3832.808	182.87	5136.174	180.78	5044.44	2.09	0.89
σ_{yy}	438.16	15324.47	406.56	11917.31	462.61	15073.42	457.20	14857.46	5.41	1.66

where

$$a^* = \left\| \frac{1}{2} (\sigma'_{PBGM} + \sigma''_{PBGM}) \right\|$$

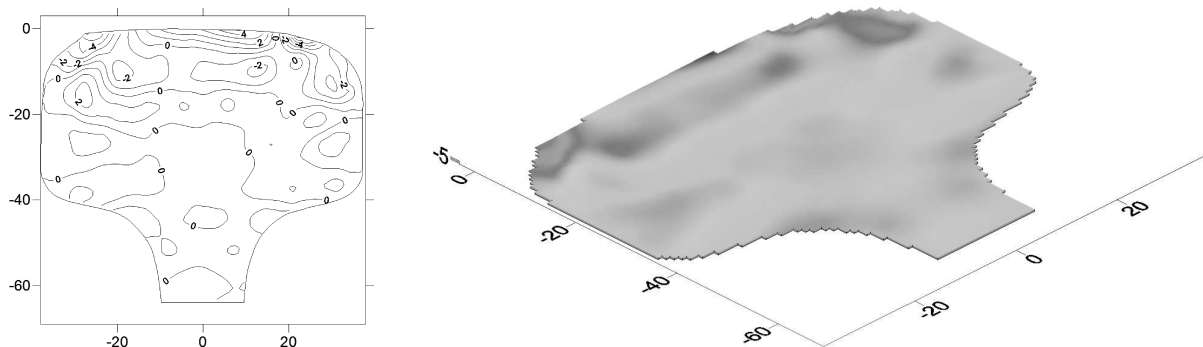
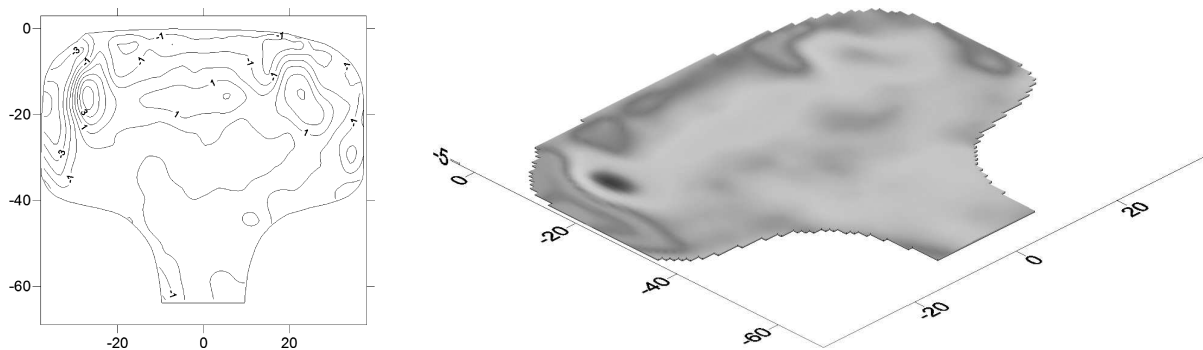
$$a^{**} = \left\| \sigma^{avg}_{PBGM} - \frac{1}{2} (\sigma'_{PBGM} + \sigma''_{PBGM}) \right\|$$

Table 4. Final error norms for T1 and T2 smoothed data.

Stress component	T1 slice data final error estimates		T2 slice data final error estimates	
	Max. [%]	L2 [%]	Max. [%]	L2 [%]
σ_{xx}	15.76	1.67	24.12	8.60
σ_{xy}	4.64	7.23	13.17	24.02
σ_{yy}	4.16	3.14	11.08	19.84

200 MPa of difference). This is not necessarily the case of the other components, because both the shear and vertical stresses show substantial decrease in the maximum and $L2$ error norms¹⁵ – but this result may be somehow puzzling. It should be stressed here that this situation does not mean that the σ_{xx} component was subject to no smoothing. It just happened that there were extreme experimental errors in the vicinity of the running tread and only by chance PBGM smoothing, which otherwise introduced a lot of corrections to the original patterns (compare e.g., the corresponding Figs. 3 and 9 or 4 and 10), ended up with values for the horizontal stress different by almost the same amount as it was before smoothing.

Analysis of the maximum and $L2$ norms for the $\Delta\bar{\sigma}'_{ij'PBGM}$ field (differences of the PBGM smoothed T1 and T2 data) in Table 2 leads to a conclusion that these fields are still different from each other by a substantial amount. This means that PBGM smoothing was not able to make them indiscernible. However, when one performs analysis of the averaged fields, the whole image changes.

**Fig. 12.** Differences between average-then-smoothen vs. smooth-then-average horizontal stresses σ_{xx} on T1 and T2 slices.**Fig. 13.** Differences between average-then-smoothen vs. smooth-then-average vertical stresses σ_{yy} on T1 and T2 slices.

¹⁵In $L2$ norm all components, including the transverse one, show decrease, even by ca. 62% like in the case of the shear stress component.

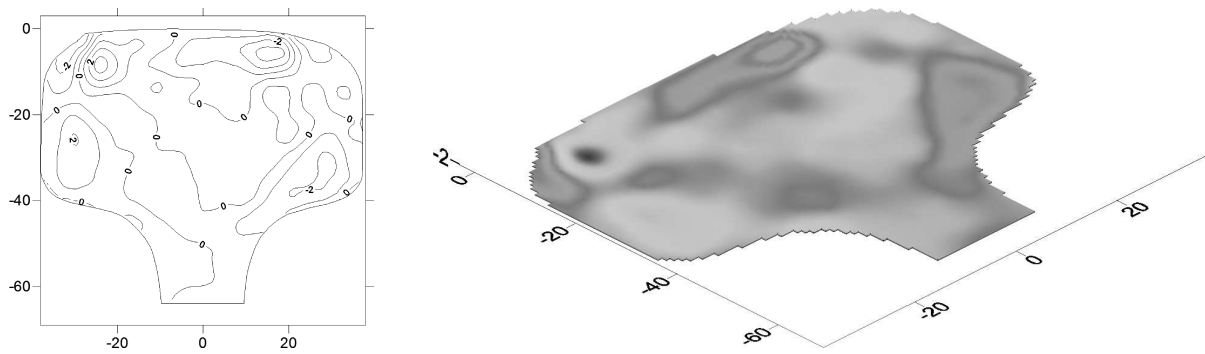


Fig. 14. Differences between average-then-smoother vs. smooth-then-average shear stresses σ_{xy} on T1 and T2 slices.

In order to perform validation of the approach with the averaged fields it is required that based on the T1 and T2 raw data sets, a virtual *Tavg* slice data set is produced and then smoothed. On the other hand, the T1 and T2 data sets are smoothed independently and their smoothed results are then averaged. When we the results of the first path (average-then-smooth) are compared with the results of the second path (smooth-then-average) and they are the same, it follows that the discrepancies between the T1 and T2 data sets were of random nature¹⁶, there is no model error and the results may be treated as credible. The results of this analysis are collected in the last two column of Table 3, where both maximum and $L2$ norms are calculated for this case. Found in ca. 5–7 MPa’s range for the maximum norm and not exceeding the value of 1.7 in case of $L2$ norm, one may be assured that now there is more than excellent agreement between the T1 and T2 data and the validity of the model was proved. The same conclusion may be drawn from the analysis of spatial distributions of functions $\mathcal{F}_1(x, y)$, $\mathcal{F}_2(x, y)$ and $\mathcal{F}_3(x, y)$. All distributions shown in Figs. 12–14 are spatially different and their amplitudes are very low – a good reason to think that there was no model error present.

5. CONCLUSIONS

The paper presented an application of PBGM method to tasks of validation of experimental procedures. The destructive nature of the experiments prevented application of the classic statistical approaches, but it was shown that physically based approximation is capable of handling these tasks with great effectiveness provided the data are collected in accordance with the new N-cut sectioning scheme. In this case, it is sufficient to provide only a single data set for each of the slices to perform “on-the-runtime” validation of the approach and to construct a posteriori error estimates of the data. All this is possible at a relatively low cost and without an excess of laboratory work.

The analysis performed for the considered rail sample showed a very good convergence of the performed PBGM smoothing processes for either the “smooth-then-average” or “average-then-smooth” strategies, with excellent reduction of error level (of ca. 2 orders as compared with the original data). This result clearly proves that the assumption of the axial direction independence of the stress state was valid. Based on the data for an additional transverse slice cut in the N-cut scheme, it was also demonstrated that the ND data may be biased by a substantial level of error, but owing to the averaging procedure it is possible to estimate and correct it.

Generally, it seems to be justified to sum the research up by a conclusion that the idea of simultaneous use of PBGM procedure and the N-cut scheme broadened the robustness of the approach and brought a new value to the previously developed methodologies.

¹⁶Averaging works as a preprocessor here and help to compensate for error before actual smoothing takes place.

REFERENCES

- [1] J. Magiera, J. Orkisz, W. Karmowski. Reconstruction of residual stresses in railroad rails from measurements made on vertical and oblique slices. *Wear*, **191**: 78–89, 1996.
- [2] C.G. Schilling, G.T. Blake. Measurement of triaxial residual stresses in railroad rails. Association of American Railroads, Chicago Technical Center, Report No. R-477, 1981.
- [3] J.J. Groom. *Determination of Residual Stresses in Rails*. Final Report for US DOT No. DOT/FRA/ORD–83/05, 1983.
- [4] Z. Świdorski, A. Wójtowicz. Plans and progress of controlled experiments on rail residual stress using the EMS-60 machine. In O. Orringer et al. [Eds.], *Residual Stresses in Rails: Effects on Rail Integrity and Railroad Economics*, Vol. I, 57–66, Kluwer Acad. Publ., Dordrecht, Boston, London, 1992.
- [5] H. Meier. Eigenspannungen in Eisenbahnschienen. *Zeitschrift Vereines Deutscher Ingenieure*, **81**(12): 362–363, 1937.
- [6] J. Magiera. *A hybrid experimental-numerical analysis of residual stress in rails*. PhD dissertation, Cracow University of Technology, Cracow, 2001.
- [7] J. Magiera. Enhanced 3D Analysis Of Residual Stress In Rails By Physically Based Fit To Neutron Diffraction Data. *Wear*, **253**, 228–240, 2002.
- [8] J. Magiera. *Enhanced setups for T/O-S experimental scheme*. Interim Report, Volpe National Transportation Systems Center, US DOT, Cambridge, MA, 2002.
- [9] W. Karmowski, J. Orkisz. A physically based method of enhancement of experimental data – concepts, formulation and application to identification of residual stresses. In: M. Tanaka, G.S. Dulikravich [Eds.], *Inverse Problems in Engineering Mechanics*. 61–70, Springer Verlag, Tokyo, 1993.
- [10] J. Magiera. A meshless FDM applied to a posteriori error analysis of experimental data by physically based global method approximation. In: K.J. Bathe [Ed.], *Computational Fluid and Solid Mechanics*, Elsevier, 2060–2063, 2003.
- [11] J. Magiera. Physically based MWLS-type approximations in smart smoothing of experimental data. In: S.M. Sivakumar et al. [Eds.], *Advances in Computational and Experimental Engineering and Sciences*, Tech Science Press, Chennai, 2005.
- [12] J. Magiera. Non-statistical physically reasonable technique for a posteriori estimation of experimental data error. *CAMES*, **13**: 593–611, 2006.
- [13] W. Karmowski, J. Orkisz. Fitting of curves and surfaces basing on interaction of physical relations and experimental data. *Appl. Math. Mod.*, **7**(65): 15–21, 1983.
- [14] J. Deputat, J. Szelązek, M. Adamski. Experiences in ultrasonic measurements of stresses in rails. In J.J. Kalker et al. [Eds.], *Rail Quality and Maintenance for Modern Railway Operation*, 109–118, Kluwer Acad. Publ., Dordrecht, Boston, London, 1993.